Saudi Journal of Biological Sciences 29 (2022) 2180–2186

Contents lists available at ScienceDirect

Saudi Journal of Biological Sciences

journal homepage: www.sciencedirect.com

Original article

Elimination of biological and physical artifacts in abdomen and brain computed tomography procedures using filtering techniques

Hiba Omer [a], Nissren Tamam [b,*], Suhaib Alameen [c], Sahar Algadi [d], Duong Thanh Tai [e], Abdelmoneim Sulieman [f,g]

[a] Department of Basic Sciences, Deanship of Preparatory Year and Supporting Studies, Imam Abdulrahman Bin Faisal University, P.O. Box 1982, Dammam 34212, Saudi Arabia
[b] Physics Department, College of Sciences, Princess Nourah bint Abdulrahman University, P.O Box 84428, Riyadh 11671, Saudi Arabia
[c] Sudan University of Science and Technology, College of Medical Radiologic Science, P.O.Box 1908, Khartoum, Sudan
[d] Department of Basic Sciences, Deanship of Preparatory Year and Supporting Studies, Imam Abdulrahman Bin Faisal University, P.O. Box 1982, Dammam 34212, Saudi Arabia
[e] Department of Industrial Electronics and Biomedical Engineering, HCMC University of Technology and Education, Ho Chi Minh 749000, Vietnam
[f] Prince Sattam Bin Abdulaziz University, College of Applied Medical Sciences, Radiology and Medical Imaging Department, PO Box 422, Alkharj 11942, Saudi Arabia
[g] Basic Science Department, College of Medical Radiologic Science, Sudan University of Science and Technology, P.O.Box 1908, Khartoum 11111, Sudan

ARTICLE INFO

Article history:
Received 29 August 2021
Revised 4 November 2021
Accepted 17 November 2021
Available online 26 November 2021

Keywords:
Biological and Physical artifacts
Computed Tomography (CT)
Image Filtering
Radiation risk

ABSTRACT

Introduction: Medical images are usually affected by biological and physical artifacts or noise, which reduces image quality and hence poses difficulties in visual analysis, interpretation and thus requires higher doses and increased radiographs repetition rate.
Objectives: This study aims at assessing image quality during CT abdomen and brain examinations using filtering techniques as well as estimating the radiogenic risk associated with CT abdomen and brain examinations.
Materials and Methods: The data were collected from the Radiology Department at Royal Care International (RCI) Hospital, Khartoum, Sudan. The study included 100 abdominal CT images and 100 brain CT images selected from adult patients. Filters applied are namely: Mean filter, Gaussian filter, Median filter and Minimum filter. In this study, image quality after denoising is measured based on the Mean Squared Error (MSE), Peak Signal-to-Noise Ratio (PSNR), and the Structural Similarity Index Metric (SSIM).
Results: The results show that the images quality parameters become higher after applications of filters. Median filter showed improved image quality as interpreted by the measured parameters: PSNR and SSIM, and it is thus considered as a better filter for removing the noise from all other applied filters.
Discussion: The noise removed by the different filters applied to the CT images resulted in enhancing high quality images thereby effectively revealing the important details of the images without increasing the patients' risks from higher doses.
Conclusions: Filtering and image reconstruction techniques not only reduce the dose and thus the radiation risks, but also enhances high quality imaging which allows better diagnosis.

1. Introduction

Computed tomography (CT) imaging contributes up to 63% of the patients' collective doses from medical exposure, leading to a significant increase in cancer incidence up to 2% (Mettler et al.,2020; Marant-Micallef et al., 2019; Brenner &Hall, 2007). Image dose is further increased with the application of contrast agents (Mututantri-Bastiyange and Chow 2020, Chow, 2021). The number of cancer incidence due to CT radiation exposure from CT procedure is increasing globally (Lumbreras et al., 2019). However, decreasing the radiation dose by reduction of exposure parameters (tube voltage (kVp) and tube current–time product

* Corresponding author.
E-mail addresses: hbomer@iau.edu.sa (H. Omer), nmtamam@pnu.edu.sa (N. Tamam), a.sulieman@psau.edu.sa (S. Alameen), saaahmed@iau.edu.sa (S. Algadi), taidt@hcmute.edu.vn (D. Thanh Tai).
Peer review under responsibility of King Saud University.

Production and hosting by Elsevier

https://doi.org/10.1016/j.sjbs.2021.11.043
1319-562X/

(mAs) will reduce the quality of the scanned images and impair the diagnostic findings (Omer et al., 2021; Sulieman et al., 2020; Alkhorayef et al., 2017). Therefore, reducing patients' radiation exposure by proper dose optimization and using up-to-date image processing techniques is recommended to reduce patient's radiation risk while maintaining diagnosable scans. (Roslee et al et al., 2020; Razali et al., February 2020), reported that patients might repeat head CT procedures up to 14 repeat exposures, and Sulieman et al reported that patients might receive approximately 140 during CT abdomen procedures (Sulieman et al., 2020; Alkhorayef et al., 2020).

Image artifacts in computed tomography is defined as inconsistency among the recreated values in a CT image. It is generally based on the material thickness and the simple geometry. Image artifacts are classically distinguished as dark or bright bands or shades There are many different types of CT artifacts: patient based, physics based and scanner based. They are also categorized as those produced due to difficulties with the CT imaging setup and the others are more sample dependent such as beam hardening, scattered radiation, and lack of x-ray infiltration. (Boas and Fleischmann, 2012, Alzain et. al 2021).

Random noise in CT decreases the image quality of CT scans and thus limits proper interpretation of the images. Noise has an unpredictable nature which may affect proper diagnosis. Eliminating it from the image poses a burden and challenge but will enhance and retrieve details of the analysis that may be hidden in the data (Anam et al., 2020; Sivakumar et al., 2014). Therefore, improvement of image quality obtained with low or regular exposure parameters by using image processing techniques without compromising image quality is recommended (Sulieman et al., 2020). It was reported that selective mean filter (SMF) can reduce the noise up to 75%, thus improve the spatial resolution of the image (Anam et al., 2020)

Image de-noising is of high importance in digital image processing, analysis and image processing applications. It is a prerequisite, especially in CT scans, which is an important method for medical imaging. De-noising of noisy or corrupted binary is done by throwing some pixels from the image and replacing them with random gray values. Several filtering methods are used to remove unwanted noise, for example, Average filtering, Gaussian filtering, Log filtering, Median filtering, Wiener filtering (Sivakumar et al., 2014).

Various image processing techniques for image optimization, restoration, retailing, and classification are reported in literature (Gonzalez & Woods, 2004; Hanselman et al., 2001; Bao, 2002; Boncelet, 2005; Baluja et al., 2013). Image noise which may appear as additive or multiplicative components need to be removed, while preserving the important signal in order to enhance and recover the analysis details that may be hidden in the data. Filtering is among the techniques that are widely used by removing the random and uncorrelated structures and retaining the resolution (Bao, 2002).

Medical imaging is defined as an instantaneous visual expression of fractional biological information of tissues of a body mainly needed to diagnose and treat diseases (Gonzalez & Woods,2002. Noise poses constraints against full benefit of the imaging facilities by corrupting the images image. Denoising may reduce the ability to visualize all details by reducing the resolution (Anam et al., 2020; Neroladaki et al., 2013; Pontana et al., 2011; Prakash et al., 2010a; Prakash et al., 2010b). Moreover, visualization depends on the skills of the radiologist, and clarity of the screen used for visualization. Numerical analysis and digital assessment of images may provide solutions for the drawbacks of image assessment by visualization. Patients got a wide range of effective doses during CT Abdomen and brain operations, according to previous studies (Sulieman et al., 2021, Abuzaid, 2021; Singh et al., 2019; Sulieman et al., 2018; Sulieman et al., 2015a)). The effective patient dosages (mSv) per procedure ranged from 0.5 mSv to 0.5–35 mSv, indicating that the patient's dose has not yet been optimized.

Limited studies are available regarding dose reduction software. Thus, reduction of patients' doses and radiogenic risk while maintaining the quality and resolution of the CT images is necessary to reduce the avoidable cancer risks. ((Prakash et al., 2010b); Pratt 2003; Jain, 2004) reported an average dose reduction of 27.7% (26.8–28.8) in chest computed tomography depending on the patients' weight using image reconstruction and filtering techniques. May (May et al 2011) reported 50% dose reduction in abdominal computed tomography.

This study aims at assessing image quality during CT abdomen and brain examinations using filtering techniques as well as estimating the radiogenic risk associated with CT abdomen and brain examinations.

2. Materials and Methods

2.1. Image acquisition

CT scans of the abdomen and brain are obtained in the axial plane of the patient for a variety of clinical indications, including trauma. Images acquisition was performed using Toshiba 64 slices (Toshiba Medical System Corporation, Japan) CT scanner at Royal Care Hospital (RCI) hospital with tube potential of 120 kVp, the current–time product was 150–225 mAs and slice thickness of 3–5 mm. The, collimation was 19–32 mm, and scan length was 11–23 cm. The data were stored in CDs as DICOM (Digital Imaging and Communications in Medicine) format and then converted to JEPG format using ImageJ image processing software. The study included 100 abdominal CT images and 100 brain CT images selected from adult patients.

The statistical parameters presented as image areas (size) and pixels values: mean, max, min and standard deviation were calculated. Images were then analyzed using ImageJ software for measurement of the image quality parameters and the results were used as input for Microsoft Excel for analysis.

Linear Filters: Linear filtering linearly combines input of the pixels with the output of their neighborhood pixels.

Mean Filters: mean filtering which can be considered as the smoothest local variation in an image, on the other hand replaces each pixel value in an image with the mean or average value of its neighbors, including itself. This allows eliminating pixel values that are unrepresentative of their surroundings. They reduce noise by inducing blurring (Sivakumar et al., 2014; Boncelet, 2005).

For calculation: let S_{xy} represent the set of coordinates in a rectangular subimage window of size$m \times n$, with its center at point (x, y). The average value of the corrupted image $g(x, y)$ in the area defined by S_{xy} is then computed to obtain a restored image whose value f at any point (x, y) is the average computed using the pixels in the region defined by S_{xy} as follows:-

$$\boldsymbol{f}(\boldsymbol{x},\boldsymbol{y}) = \frac{1}{\boldsymbol{mn}} \sum_{(\boldsymbol{s},\boldsymbol{t})\in \boldsymbol{Sxy}} \mathbf{g}(\mathbf{s},\mathbf{t}) \quad (1)$$

Gaussian filters*:* The Gaussian filtering detects peaks that are to be impulses. This filter corrects all the amplitude spectrum coefficients within the filter window rather than the spectral coefficient of interest only (Baluja et al., 2013).

Non– linear filters: Non-linear filters reduces noise while preserving edges that are commonly blurred while using linear filters.

Median Filters: In median filter the intensity or brightness level are basically considered for ranking of the neighboring pixels. The value of the pixel being evaluated is then replaced by the median

value of pixel of interest and surrounding pixel values, as illustrated in equation (2) ((Sivakumar et al., 2014; Boncelet, 2005).

$$\boldsymbol{f}(\boldsymbol{x}) = \boldsymbol{median}_{(\boldsymbol{s},\boldsymbol{t})\in \boldsymbol{S}\boldsymbol{x}\boldsymbol{y}}\{\mathbf{g}(\mathbf{s},\mathbf{t})\} \quad (2)$$

These filters are very useful in the presence of both bipolar and unipolar impulse noise.

Minimum filters: These are very effective in detecting the darkest point in an image. They are also useful in reducing salt noise as a result of the min operation (equation (3)) (Boncelet, 2005):

$$\boldsymbol{f}(\boldsymbol{x}) = \boldsymbol{min}_{(\boldsymbol{s},\boldsymbol{t})\in \boldsymbol{S}\boldsymbol{x}\boldsymbol{y}}\{\mathbf{g}(\mathbf{s},\mathbf{t})\} \quad (3)$$

2.2. Image quality evaluation metrics

Mean Square Error (MSE): The signal fidelity measure used in MSE quantitively compares two signals by describing the degree of similarity and the level of distortion between the signals processed. Comparison is performed by assuming that one of the signals is a pristine original, while the other is distorted as a result of noise (Goyal & Sekhon, 2011). The MSE is defined as illustrated in equation (4):

$$\mathbf{MSE} = \frac{1}{\boldsymbol{NM}}\sum_{\boldsymbol{i}=1}^{\boldsymbol{N}}\sum_{\boldsymbol{j}=1}^{\boldsymbol{M}}\{\boldsymbol{I}_{\boldsymbol{original}}(\boldsymbol{i},\boldsymbol{j}) - \boldsymbol{I}_{\boldsymbol{denoised}}(\boldsymbol{i},\boldsymbol{j})\}^2 \quad (4)$$

Where, N, M: give the size of the image.

$\boldsymbol{I}_{\boldsymbol{original}}$i is the pixel values at location (i, j) of the original, unprocessed image

$\boldsymbol{I}_{\boldsymbol{denoised}}$iis the pixel values at location (i, j) of the denoised image.

Peak Signal-to-Noise-Ratio (PSNR) calculates the ratio between the maximum possible power of a signal (peak signal) and the power of corrupting noise affecting its fidelity. PSNR is quite often expressed in logarithmic decibel scale (Napoleon, D. & Praneesh, 2013).

The PSNR computes as:

$$\mathbf{PSNR} = 20\boldsymbol{log}_{10}\frac{255^2}{\boldsymbol{MSE}} \quad (5)$$

Where MSE refers to the mean square error estimated between the original and denoised images.

Structural Similarity Index Metric (SSIM): The SSIM index compares and contrasts two images. It is a full reference metric that performs calculation based on an initial distortion-free image as reference (Hore & Ziou, 2010). SSIM is a combination of factors: contrast distortion, luminance distortion and loss of correlation.

$$SSIM(f,g) = l(f,g)c(f,g)s(f,g)$$

$$\boldsymbol{l}(\boldsymbol{f},\boldsymbol{g}) = \frac{2\boldsymbol{\mu}_f\boldsymbol{\mu}_g + \boldsymbol{c}_1}{\boldsymbol{\mu}_f^2 + \boldsymbol{\mu}_g^2 + \boldsymbol{c}_1}\boldsymbol{c}(\boldsymbol{f},\boldsymbol{g}) = \frac{2\boldsymbol{\sigma}_f\boldsymbol{\sigma}_g + \boldsymbol{c}_2}{\boldsymbol{\sigma}_f^2 + \boldsymbol{\sigma}_g^2 + \boldsymbol{c}_2}\boldsymbol{s}(\boldsymbol{f},\boldsymbol{g}) = \frac{2\boldsymbol{\sigma}_{\boldsymbol{fg}} + \boldsymbol{c}_3}{\boldsymbol{\sigma}_f\boldsymbol{\sigma}_g + \boldsymbol{c}_3} \quad (6)$$

The luminance comparison function $\boldsymbol{l}(\boldsymbol{f},\boldsymbol{g})$ measures the adjacency of the mean luminance of the images ($\boldsymbol{\mu}_f$*and*$\boldsymbol{\mu}_g$). This factor has a maximum value of 1 only if$\boldsymbol{\mu}_f$=$\boldsymbol{\mu}_g$.

The contrast comparison function $\boldsymbol{c}(\boldsymbol{f},\boldsymbol{g})$ measures the proximity of the contrast of the two images. It is measured by the standard deviation values: $\boldsymbol{\sigma}_f$ and $\boldsymbol{\sigma}_g$. This factor has a maximum value of 1 only if$\boldsymbol{\sigma}_f$ = $\boldsymbol{\sigma}_g$.

The structure comparison function $\boldsymbol{s}(\boldsymbol{f},\boldsymbol{g})$ computes the correlation coefficient between the two images f and g $\boldsymbol{\sigma}_{\boldsymbol{fg}}$ is the covariance between f and g.

The SSIM values are in the range (0,1) where 0 indicates that there is absolutely no correlation between images, and 1 indicates that f is exactly the same as g. The positive constants $\boldsymbol{c}_1$, $\boldsymbol{c}_2$ and $\boldsymbol{c}_3$ are used to avoid a null denominator (Hore & Ziou, 2010).

Visual assessment by a radiologist to compare the original and filtered images.

ImageJ Software: ImageJ, a development from NIH Image, is a free-to-download image analysis program with hundreds of built-in free routines. This provides a plugin framework for adding custom functionality.

Procedure of the program: CT images with DICOM format of abdomen and brain were used for this study. Fig. 1 shows ImageJ software window

Some filters: Mean filter, Gaussian filter, Median filter, and Minimum filter were for de-noising the above images. In order to restore the noisy images, de-noising techniques were used with IMAGEJ programming. At the first stage, images of DICOM format were converted to JPEG format using ImageJ programming. At the second stage, different types of filters were applied using ImageJ software to remove noise from all CT images. At the final stage, the result of using all filters applied on CT images was compared, by using image quality parameters such as: MSE, SSIM and PSNR for all images with a main goal of deciding the best CT images denoising filters.

So, the first step is to open the image/images for comparison. The steps are: File --> open

For choosing the type of filter the steps are: Process --> filters, then choose the type of filter

For comparison of MSE between the original and denoised image: Process --> image calculator

For comparison of SSIM between the origin and denoised image: Plugins --> SSIM Index

2.3. CT brain and abdomen effective dose estimation

Dose descriptors were recorded per procedures (DLP, (mGy.cm) and per slice (CTDIvol, mGy) from a calibrated CT machine. The effective dose (E) in mSv per CT procedure obtained using CTDOSE software, based on the following equations:

The Mean effective tube current–time product (also referred to as effective mAs) was calculated for each anatomic region using:

$$effectivemAs = \frac{current(mA) \times rotationtime(s)}{beampitch} \quad (7)$$

volume Computed Tomography Dose Index $(CTDI)_{vol}$ for each anatomic region was calculated using:

$$CTDI_{vol} = effectivemAs \times constant \quad (8)$$

The constant in equation (2), determined by imaging dosimetry phantoms with the same tube voltage and the same beam width is provided by the vendor. The constant for the head and neck where obtained using a 16 cm phantom. That for chest, abdomen, pelvis, and proximal thigh was a 32 cm phantom

$CTDI_{vol}$ was converted to DLP using:

$$DLP = CTDI_{vol} \times scanlength \quad (9)$$

The regional effective dose (ED) was determined using the DLP for each region by:

$$Equivalentdose = DLP \times conversionfactor \quad (10)$$

Following ICRP publication (ICRP 103, 2007), the conversion factors was defined as 0.0021, and 0.015 mSv/mGy/cm for the brain and abdomen respectively

2.4. Radiation risk estimation

The radiation induced cancer risks per CT head and abdomen procedures were calculated by multiplying the patients' effective

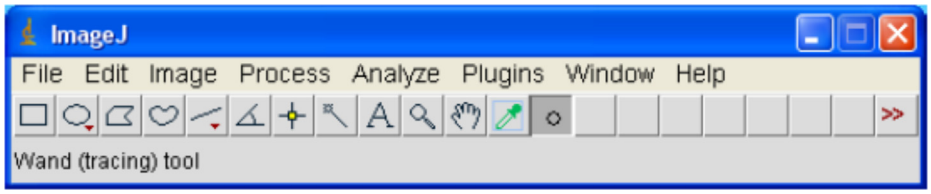

Fig. 1. ImageJ software window.

dose (mSv) from entire procedures (head & abdomen) by the cancer risk factor of 5.5×10^{-2} Sv^{-1} for a general population as a result of ionizing radiation exposure (ICRP 103, 2007).

$$E(mSv) = \sum W_{T\times}H_T \tag{11}$$

where

H_T is the equivalent dose and W_T tissue weighting factor

3. Results

In our study, we used 100 abdomens and 100 brains CT scan images in DICOM format at Royal Care International (RCI) Hospital. Each slice of images had the size of 512 X 512. ImageJ, a flexible and extensible data model, was used to provide digital analysis of the images and the results were compared with visual assessment for the original and filtered images. ImageJ provides a user interface with functions to load, display, and save images; basic image-processing functionality, such as convolution filters; and an extension mechanism including support for plugins and macros that tap into functionality to provide recording, replaying and thus automate image processing workflow that is re-usable and easy to teach or demonstrate (Schindelin et al., 2015). It also allows to connect to external toolkits without the need to export and open files (Schneider et al., 2012).

The following filters: Minimum, Gaussian, Median, and Mean were used on the original images (abdomen and brain) to remove noise. Fig. 2 shows different linear and Non-Linear Filters Applied for abdominal CT scan images.

Fig. 3 shows different linear and non-linear filters applied for brain CT scan images.

4. Discussion

CT artifacts are common and can degrade image quality. Due to the resemblance of these artifacts to the anatomy and pathology, it is very crucial to identify and eliminate them. CT artifact, which are mainly classified according to the underlying cause of the artifact, refers to any systematic differences between the CT numbers in the reconstructed image and the actual attenuation coefficients of the object. CT artifacts are generally divided into three categories: Physics-based artifacts due to faults in image acquisition, patient-based artifacts which are commonly interpreted as misregistration artifacts appearing as blurring, streaking, or shading within the image and scanner-based artifacts, which result from malfunction or imperfection of the scanners.

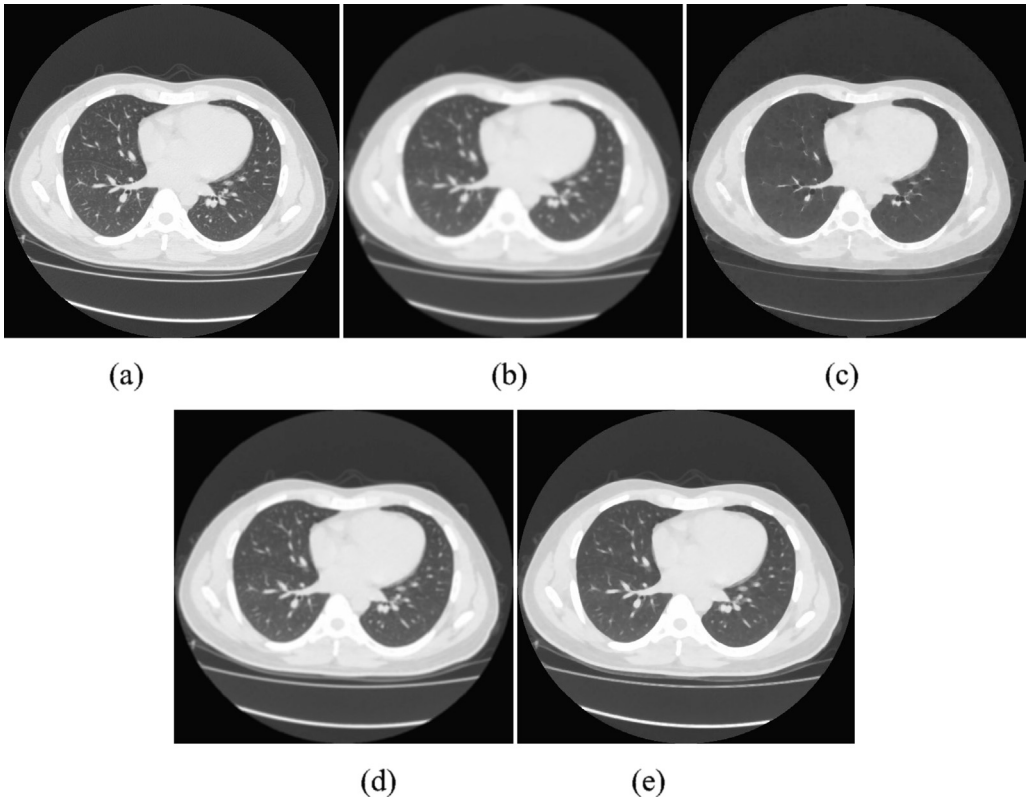

Fig. 2. Abdominal CT scan images without (a) and with the filters (b).

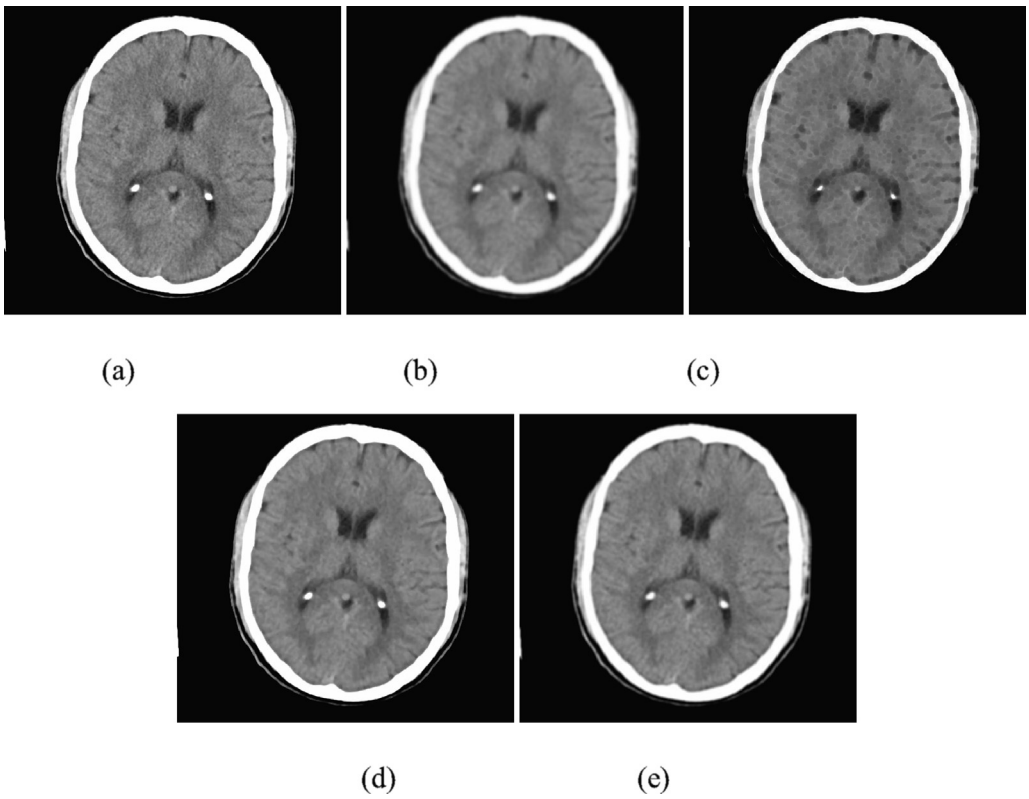

Fig. 3. Brain CT scan images without (a) and with the filters (b).

The most important form of physics-based artifacts is beam hardening which occurs when an x-ray beam comprised of polychromatic energies passes through an object, resulting in selective attenuation of lower energy photon. It has two distinct manifestations, streaking (dark bands) and cupping. Other physics-based artifacts include (but are not limited to) metal artifact/high-density foreign material artifact, partial volume averaging, quantum mottle (noise), photon starvation, ring artifacts, out of field artifacts and air bubble artifacts

Patient-based artifacts are caused by: involuntary or voluntary motion of the patient, clothing, jewelry, dental or metal prothesis or orthosis.

Scanner-based artifacts include ring and wobble artifacts. (Boas and Fleischmann, 2012, Alzain et. al 2021).

Upon visualization of the images for the different scans pre-and post-denoising, the radiologist's comments and feedback was as follows: In Fig. 2 the lung parenchyma and broncho-vascular markings showed better contrast and special resolution in image (a) without filter than other images (b, c, d and e) with different applied filters. The difference was not very large, especially between Median and mean filtered images; where Mean filters showed better details. The size of screen used to visualize and assess the images played a major role; using a smaller screen, many details were lost.

In Fig. 3 the gray white matter differentiation, the basal ganglia and internal capsule were better evaluated in the original image (a) than the images with applied filters. However, when comparing the different types of filters, the Mean filter showed the best resolution, followed by the Median filter

The applied filters had different abilities in removing noise. Median filter proved to have higher capabilities in noise reduction. This is reflected by the image quality parameters of MSE, SSIM and PSNR in dB. Median filter showed minimum value of MSE and maximum values of SSIM and PSNR after applied on both abdomen and brain CT images as shown on Table 1.

Fig. 4 displays graphical representation of the MSE, PSNR and SSIM outputs of each filter for the abdomen CT

Fig. 5 displays graphical representation of the MSE, PSNR and SSIM outputs of each filter for the brain CT

Therefore, we studied the image filtering methods for abdomen CT scan and brain CT scan images by assessing the comparison different parameters. It is evident that applying filters have different abilities in removing noise from both abdomen and brain CT scan images. Median filter performed very well in terms of noise reduction compared with the other filtering methods. It provides the maximum PSNR, SSIM and minimum MSE. Sivakumar & Chandrasekar studied image filters for noise reduction in lung CT images, by using namely Mean filter, Wiener filter, Median filter and Entropy filter (Sivakumar & Chandrasekar, 2014). In results they found clearly that Wiener filter performs very well compared to the other filtering methods. Moreover, the Median filter also performs better than the Mean filter, as is presented in this study. So, median filters reduce noise from CT images far better than mean filter without specifying the type of noise in images. This is in contrast with the visual assessment where the original unfiltered image was the best in terms of providing details, followed by the Mean filter and then, the Median filter.

Table 2 shows the patients' doses per CT abdomen and brain procedures and the relevant radiation risk. The results showed that this dose is high compared to previous studies reported by (Omer et al., 2021; Sulieman et al., 2015a, 2018; Suliman et al., 2015b). The risk for abdomen procedures is more increased than brain procedures because CT abdomen usually is a multi-phasic procedure with extended scan length. Many sensitive organs are included in the primary beam. Therefore, improving the image quality in this study enables operators to use the lowest exposure parameters

Table 1
Image Quality Measures for Both the Linear and Non-Linear Filters applied on abdomen and brain CT scan Images.

Image quality Measures		Abdomen CT filtered images (Average Value of 100 Images)			Brain CT filtered images (Average Value of 100 Images)		
		MSE	PSNR	SSIM	MSE	PSNR	SSIM
Linear filters	Mean	10.2	38.26	0.96	8.17	39.41	0.98
	Gaussian	14.46	36.66	0.93	12.95	37.32	0.95
Non–linear filters	Median	4.82	41.54	0.98	3.05	44.52	0.99
	Minimum	47.02	31.55	0.81	38.53	32.78	0.87

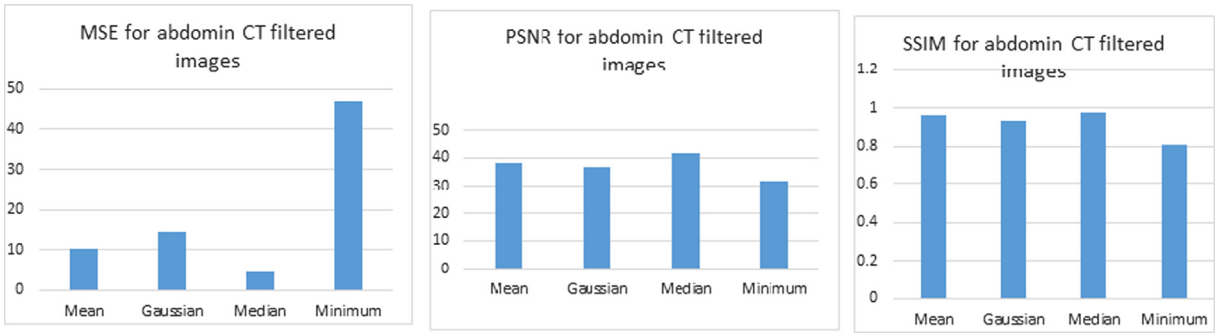

Fig. 4. Graphical representation of the MSE, PSNR and SSIM outputs of each filter for the abdomen CT.

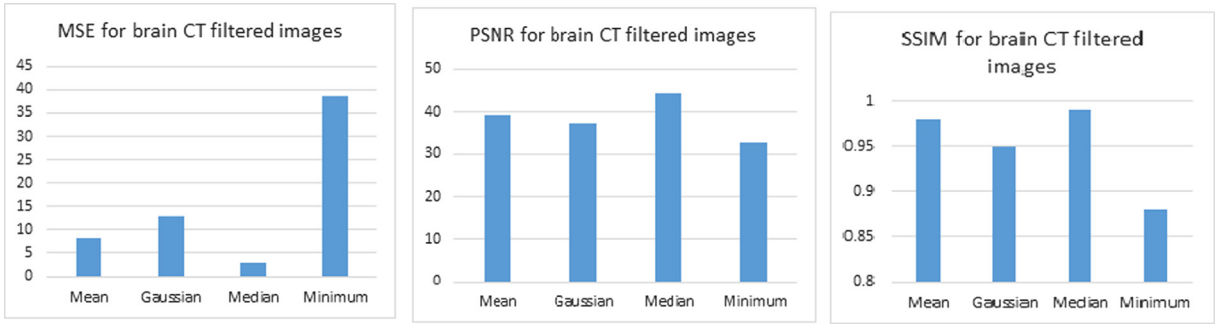

Fig. 5. Graphical representation of the MSE, PSNR and SSIM outputs of each filter for the brain CT.

Table 2
Patients' effective dose during CT brain and abdomen.

Organ	CTDIvol (mGy)	DLP (mGy.cm)	Effective dose (mSv)	Average radiation risk per 10^4 procedures
Brain	74.9 ± 10 (48.0–80.8)	1387.9 ± 223 (700.7–1549.8)	2.9 ± 0.5 (1.5–3.3)	2
Abdomen	70.3 ± 22 (28.5–95.4)	1483.0 ± 678 (710.2–3602.8)	22.4 ± 10.2 (10.7-)	12

to obtain a diagnosable scan with minimal patient risk. The probability of developing radiogenic cancer as a result of a patient's radiation exposure is dependent on a number of factors, all of which are sources of uncertainty. Age at exposure, the amount of radiation dose, and the affected organ are all considerations to consider. It's worth noting that over 98 percent of cancer cases are thought to be caused by factors other than ionizing radiation exposure (Mettler et al., 1995). In general, the risk rises in direct proportion to the patient's age, and the higher the absorbed dose, the more likely a biological effect would be noticed.

5. Conclusions

CT imaging is very useful in diagnosis of diseases. Unfortunately, they are often distorted by biological and physical artifacts which reduces the quality of images. Visual assessment of the images is quite subjective especially with the presence of noise. Digital or numeric assessment provides a better tool for image interpretation and allows surpassing of the effects of noise.

This study used different filters and different image quality parameters, namely: Mean filter, Gaussian filter, Median filter, and Minimum filter compared the image filtering methods for abdomen CT scan and brain CT scan images. Applying filters played a role in removing noise from both abdomen and brain CT scan images. Nevertheless, it reduces the resolution and thus the visualization of the image. Median filters performed very well in terms of noise reduction compared with the other filtering methods but blurred the original images. Nevertheless, the organs were still visible to the radiologist. Median filters also proved effective in terms of digital analysis of denoised images which seemed to be distorted and of poor quality during visual assessment. This is achieved by providing the maximum PSNR, SSIM and minimum MSE.

Filtering and image reconstruction techniques not only reduce the dose and thus, the radiation risks, but also enhances high quality imaging which allows better diagnosis. The use of the filters is thus recommended for further patients' dose reduction without deteriorating the image quality. Being accompanied with digital analysis, they can allow better interpretation of images and prevents human errors in visual assessment of images, and are thus recommended by this study instead of the subjective human visualization and assessment. Performing filtering to reduce double losses of data is recommended to decrease the gap between visualization and numeric analysis.

Declaration of Competing Interest

The authors declare that they have no known competing financial interests or personal relationships that could have appeared to influence the work reported in this paper.

Acknowledgment

The authors express their gratitude to Princess Nourah bint Abdulrahman University Researchers Supporting Project (Grant No. PNURSP2022R12), Princess Nourah bint Abdulrahman University, Riyadh, Saudi Arabia.

References

Abuzaid, M.M., Elshami, W., Tekin, H.O., Sulieman, A., Bradley, D.A., 2021. Comparison of Radiation dose and Image Quality in Head CT Scans Among Multidetector CT Scanners ncab125 Radiat. Prot. Dosim. https://doi.org/10.1093/rpd/ncab125.

Alkhorayef, M., Sulieman, A., Barakat, H., Al-Mohammed, H., Theodorou, K., Kappas, C., Bradley, D., 2020. Urethrographic examinations: Patient and staff exposures and associated radiobiological risks. Saudi J. Biol. Sci. 28 (1), 35–39.

Alkhorayef, M., Babikir, E., Alrushoud, A., Al-Mohammed, H., Sulieman, A., 2017. Patient radiation biological risk in computed tomography angiography procedure. Saudi J. Biol. Sci. 24 (2), 235–240.

Alzain, A., Elhussein, N., Fadulelmulla, I., Ahmed, A., Elbashir, M., Elamin, B., 2021. Common computed tomography artifact: source and avoidance. Egypt. J. Radiol. Nucl. Med. 52 (1), 151.

Anam, C., Adi, K., Sutanto, H., Arifin, Z., Budi, W.S., Fujibuchi, T., Dougherty, G., 2020. Noise Reduction in CT Images Using a Selective Mean Filter. J. Biomed. Phys. Eng. 10 (5), 623–634.

Baluja, Y., Mishra, S., Saini, T.S., Pati, M.V., 2013. Frequency Domain Based Data Hiding Technique for Audio Signal. Int. J. Innovative Res. Sci. Eng. Technol. 2 (5), 1564–1569.

Bao, S.L.M., 2004. medical imaging physics. Medical Publishing House of Beijing University.

Boas, F.E., Fleischmann, D., 2012. CT artifacts: Causes and reduction techniques. Imaging Med. 4 (2), 229–240.

Boncelet, C., 2005. Image noise models. Elsevier Academic Press, UK, Handbook of image and video processing, pp. 325–335.

Brenner, D., Hall, E., Phil, D., 2007. Computed Tomography — An Increasing Source of Radiation Exposure. New England J. Med. 357, 2277–2284.

Chow J., 2021. Evaluation of the risk and benefit of using functionalized nanomaterials as contrast agents in image-guided radiotherapy: A Monte Carlo study on the imaging dose and contrast enhancement. Chapter 12, Handbook of Functionalized Nanomaterials. Elsevier Inc.

Gonzalez, R.C., Woods, R.E., 2002. Digital Image Processing. Prentice Hall, Upper Saddle River, NJ.

Gonzalez, R., Woods, R., Eddins, S. 2004. Digital Image Processing using MATLAB", Pearson Education, 2004, Chapter 10, 378 – 425.

Goyal, M., Sekhon, G.S., 2011. Hybrid Threshold Technique for Speckle Noise Reduction using wavelets for Grey scale images. Int. J. Image Graphics Sig. Process. (IJIGSP) 2 (2), 620–625.

Hanselman, D., Littlefield, B.R., 2001. Mastering MATLAB 6. Prentice Hall, Upper Saddle River, NJ.

Hore, A., Ziou, D., 2010. Image quality metrics: PSNR vs. SSIM. In: In: Pattern recognition (icpr), 2010 20th international conference on, pp. 2366–2369.

ICRP 103, 2007. The 2007 Recommendations of the International Commission on Radiological Protection, The International Commission on Radiological Protection, 2007. Annual of ICRP. 37(2-4):1-332.

Jain, A., 2004. Fundamentals of Digital Image Processing Chapter 9. Prentice Hall of India, pp. 342–430.

Lumbreras, B., Salinas, J.M., Gonzalez-Alvarez, I., 2019. Cumulative exposure to ionising radiation from diagnostic imaging tests: a 12-year follow-up population-based analysis in Spain. BMJ Open 9 (9), e030905. https://doi.org/10.1136/bmjopen-2019-030905.

Marant-Micallef, C., Shield, K.D., Vignat, J., et al., 2019. The risk of cancer attributable to diagnostic medical radiation: estimation for France in 2015. Int. J. Cancer 144 (12), 2954–2963.

May, M., Wust, W., Brand, M., Stahl, C., Allmendinger, T., Schmidt, B., Uder, M., Lell, M., 2011. Dose Reduction in Abdominal Computed Tomography. Intraindividual Comparison of Image Quality of Full-Dose Standard and Half-Dose Iterative Reconstructions with Dual-Source Computed Tomography. Investigative Radiol. 46 (7), 465–470.

Mettler, F., Mahesh, M., Bhargavan-Chatfield, M., Chambers, C., Elee, J., Frush, D., Miller, D., Royal, H., Milano, M., Spelic, D., Ansari, A., Bolch, W., Guebert, G., Sherrier, R., 2020. Patient Exposure from Radiologic and Nuclear Medicine Procedures in the United States: Procedure Volume and Effective Dose for the Period 2006–2016. Radiology 295, 418–427.

Mettler, F.A., Upton, A.C., 1995. Medical Effects of Ionizing Radiation. WB Saunders Co., Philadelphia.

Mututantri-Bastiyange, D., Chow, J., 2020. Imaging dose of cone-beam computed tomography in nanoparticle-enhanced image-guided radiotherapy: A Monte Carlo phantom study. AIMS Bioeng. 7 (1), 1–11.

Napoleon, D., Praneesh, M., 2013. Detection of Brain Tumor Using Kernel Induced Possiblistic C-Means Clustering. Int. J. Comput. Organization Trends 3 (9), 436–438.

Neroladaki, A., Botsikas, D., Boudabbous, S., Becker, C.D., Montet, X., 2013. Computed tomography of the chest with model-based iterative reconstruction using a radiation exposure similar to chest X-ray examination: preliminary observations. Eur. Radiol. 23 (2), 360–366.

Omer, H., Alameen, S., Mahmoud, W., Sulieman, A., Nasir, O., Abolaban, F., 2021. Eye lens and thyroid gland radiation exposure for patients undergoing brain computed tomography examination. Saudi J. Biol. Sci. 28 (1), 342–346.

Pontana, F., Pagniez, J., Flohr, T., Faivre, J.B., Duhamel, A., Remy, J., Remy-Jardin, M., 2011. Chest computed tomography using iterative reconstruction vs filtered back projection (Part 1): Evaluation of image noise reduction in 32 patients. Eur. Radiol. 21 (3), 627–635.

Prakash, P., Kalra, M.K., Digumarthy, S.R., Hsieh, J., Pien, H., Singh, S., Gilman, M.D., Shepard, J.A., 2010a. Radiation dose reduction with chest computed tomography using adaptive statistical iterative reconstruction technique: initial experience. J. Comput. Assist. Tomogr. 34 (1), 40–45.

Prakash, P., Kalra, M.K., Kambadakone, A.K., Pien, H., Hsieh, J., Blake, M.A., Sahani, D. V., 2010b. Reducing abdominal CT radiation dose with adaptive statistical iterative reconstruction technique. Invest. Radiol. 45 (4), 202–210.

Pratt, W., att 2003. Digital Image processing 2nd ed. Chapter 17. Wiley-Interscience Publication, pp. 551–558.

Razali, M.A.S.M., Ahmad, M.Z., Shuaib, I.L., Osman, N.D., February 2020. Optimization of radiation dose in ct imaging: establishing the institutional diagnostic reference levels and patient dose auditing. Radiat. Prot. Dosim. 188 (2), 213–221.

Roslee, M., Shuaib, I., Napi, A., Razali, M., Osman, N., 2020. Cumulative organ dose and effective dose in adult population underwent repeated or multiple head CT examination. Radiat. Phys. Chem. 166, 108465. https://doi.org/10.1016/j.radphyschem.2019.108465.

Schindelin, J., Rueden, C., Hiner, M., Eliceiri, K., 2015. The ImageJ Ecosystem: An Open Platform for Biomedical Image Analysis. Mol. Reprod. Dev. 82 (7-8), 518–529.

Schneider, C., Rasband, W., Eliceiri, K., 2012. NIH Image to ImageJ: 25 years of image analysis. Nat. Methods 9 (7), 671–675.

Singh, R., Szczykutowicz, T.P., Homayounieh, F., Vining, R., Kanal, K., Digumarthy, S. R., Kalra, M.K., 2019. Radiation Dose for Multiregion CT Protocols: Challenges and Limitations. AJR Am. J. Roentgenol. 213 (5), 1100–1106.

Sivakumar, S., Chandrasekar, C., 2014. A Comparative study on image filters for noise reduction in lung CT scan images. IJCSEITR 4, 243–250.

Sulieman, A., Tammam, N., Alzimami, K., Elnour, A.M., Babikir, E., Alfuraih, A., 2015a. Dose reduction in chest CT examination. Radiat. Prot. Dosimetry. 165 (1–4), 185–189.

Sulieman, A., Elnour, A., Mahmoud, M., Alkhorayef, M., Hamid, O., Bradley, D., 2020. Diagnostic reference level for computed tomography abdominal examinations: A multicentre study. Radiat. Phys. Chem. 174, 108963.

Sulieman, A., Adam, H., Elnour, A., Tamam, N., Alhaili, A., Alkhorayef, M., Alghamdi, S., Mayeen, Uddin K., Bradley, D., 2021. Patient radiation dose reduction using a commercial iterative reconstruction technique package. Radiat. Phys. Chem. 178, 108996.

Suliman, I., Khamis, H., Ombada, T., Alzimami, K., Alkhorayef, M., 2015b. Radiation exposure during paediatric CT in Sudan: CT dose, organ and effective doses. Radiat. Prot. Dosim. 167 (4), 513–518.

Sulieman, A., Mahmoud, M.Z., Serhan, O., Alonazi, B., Alkhorayef, M., Alzimami, K., Bradley, D., 2018. CT examination effective doses in Saudi Arabia. Appl. Radiat. Isot. 141, 261–265.